remote sensing

MDPI

Letter

Are There Sufficient Landsat Observations for Retrospective and Continuous Monitoring of Land Cover Changes in China?

Yan Zhou [1,2], Jinwei Dong [2,*], Jiyuan Liu [2], Graciela Metternicht [3], Wei Shen [1], Nanshan You [2], Guosong Zhao [2], Xiangming Xiao [4]

[1] School of Earth Sciences and Resources, China University of Geosciences, Beijing 100083, China
[2] Key Laboratory of Land Surface Pattern and Simulation, Institute of Geographic Sciences and Natural Resources Research, Chinese Academy of Sciences, Beijing 100101, China
[3] School of Biological, Earth and Environmental Sciences, University of New South Wales, Sydney, NSW 2052, Australia
[4] Department of Microbiology and Plant Biology, and Center for Spatial Analysis, University of Oklahoma, Norman, OK 73019, USA
* Correspondence: dongjw@igsnrr.ac.cn; Tel.: +86-10-6488-8827

Received: 12 June, 2019; Accepted: 29 July 2019; Published: 1 August 2019

Introduction

The supplementary material includes the following contents: (1) The yearly and monthly numbers of Landsat imagery in China from 1984 to 2017; (2) the yearly and monthly average numbers of total and valid Landsat observations in China from 1984 to 2017; (3) spatial distributions of total and valid Landsat observations in China in different months; (4) spatial distributions of total and valid Landsat observations in China in terms of different sensors; (5) Google Earth Engine codes for the investigations of Landsat data availability in China.

Text S1. Yearly and Monthly Numbers of Landsat Imagery in China

Figure S1 shows the yearly and monthly amounts of L5/7/8 surface reflectance images in China during 1984–2017. The yearly and monthly amounts of Landsat images generally show an increasing trend over time, with two sharp increases during 1999–2000 and 2013–2014 (Figures S1a and S1b). The yearly amounts of Landsat images increased from ~5000 images/year before 1999 to ~10,000 images/year during 2000–2011, then they decreased in 2012, followed by a dramatic increase to ~15,000 images/year since 2013 (Figure S2a). In terms of the three sensors, the yearly amount of images of L8 were the most (7047–10,005), followed by those from L7 (1731–8871) and L5 (576–8318). The monthly amounts of Landsat images increased from ~500 images/month before 1999 to ~1000 images/month during 2000–2011, then they decreased in 2012, followed by a dramatic increase to ~1500 images/month since 2013 (Figure S1b).

Figure S2 shows the monthly amounts of L5, 7, and 8 images in China from 1984 to 2017, respectively. For L5, the yearly amount of images gradually increased since 1984, and has kept relatively stable since 1991 (Figure S2a). Significant variations exist in monthly L5 image numbers among different months, ranging from 0 to 856. For L7, the monthly amounts of images have gradually increased since July 1999, and kept relatively stable since 2000 (Figure S2b). The numbers of L7 images also vary among different months, ranging from 0 to 865. It was obvious in the color intensity map that the monthly amounts of L7 images during 2014–2017 were significantly more than those in the previous years (Figure S2b). For L8, the differences in monthly amounts of images were smaller compared to L5 and L7, ranging from 143 to 914 (Figure S2c). In terms of the comparisons among the three sensors, the monthly amounts of images from L8 were the highest (ranging from 143 to 914), followed by L7 (0 to 865), and L5 (0 to 856) (Figures S2a–S2c).

Text S2. Yearly Average Numbers of Total and Valid Landsat Observations in China

Figure S3 shows the yearly average number of total and valid observations of the three Landsat sensors in China from 1984 to 2017. As can be seen, the annual average number of total (valid) observations of the three Landsat sensors within China varied from 1.63 to 60.25/1.13 to 31.72 during 1984–2017 (Figures S3a and S3b). Specifically, the annual average number of total (valid) Landsat observations gradually increased after the launch of L5 in March 1984, and kept relatively stable to ~20 (~10) from 1991 (Figures S3a and S3b). Then, the numbers increased from 1999, and reached ~40 (~20) since 2000, double of what they were during 1991–1999 (Figures S3a and S3b). Due to the failure of L5 in capturing images since November 2011, the annual average numbers of total (valid) observations decreased to ~20 (~10) in 2012. With the launch of L8 in February 2013, the numbers dramatically increased from 2013, and have kept relatively stable to ~60 (~30) since 2014 (Figures S3a and S3b). In terms of the three sensors, the annual average numbers of total (valid) observations within China from L8 were the most, ranging from 22.75 to 32.67 (13.38 to 18.77), followed by L7 (5.31 to 27.63/3.52 to 13.37), and L5 (1.63 to 25.73/1.13 to 15.50).

Text S3. Spatial Distributions of Total Landsat Observations in China in Different Months

Figure S4 shows the spatial distributions of total Landsat observations within China in different months. Generally, total Landsat observations in China in January–April showed similar spatial patterns, namely: The central, southern, and western parts of China had relatively less observations with numbers less than 100, while there were more observations with numbers more than 100 in the northern and southwestern parts of China (Figure S4). Then, the total observation numbers in Southwestern China began to decrease in May, and only Northern and Northeastern China had relatively more observations with numbers more than 100 in June (Figure S4). From July, the observation numbers in the eastern parts of China began to increase, and Landsat observations across the entirety of China showed similar spatial patterns in July and August, namely: Northern and Eastern China had relatively more observations with numbers more than 100, while Western and Southwestern China had less observations with numbers less than 100 (Figure S4). After that, the total observation numbers in the southwestern parts of China began to increase from September (Figure S4), and the spatial patterns of Landsat observations in China were similar in October–December, namely: Southern China had relatively less observations, as well as the western parts of the Xinjiang Autonomous Region and the northern parts of the Tibet Autonomous Region; while Northern, Northeastern, Eastern, and Southwestern China had more observations (Figure S4).

To reveal the spatial patterns of Landsat observations along with latitudes (15 N°–50 N°), we also calculated the average number of total observations in each one-degree latitude interval within China. Generally, the average numbers of total observations in each one-degree latitude interval within China increased along with the latitudes, though it showed a decreasing trend along with the latitudes in high latitudes (>45 N°) in December and January (Figure S4).

Text S4. Spatial Distributions of Valid Landsat Observations in China in Different Months

Figure S5 shows the spatial distributions of valid Landsat observations within China in different months. Generally, valid Landsat observations in China in January–April showed similar spatial patterns, namely: The central, southern, and western parts of China had relatively less valid observations with numbers less than 80, while there were more valid observations with numbers more than 80 in the northern and southwestern parts of China. Then, the valid observation numbers in Southwestern China began to decrease in May, and only Northern and Northeastern China had relatively more valid observations with numbers more than 80 in June. From July, the valid observation numbers in the eastern parts of China began to increase, and valid Landsat observations across the entirety of China showed similar spatial patterns in July and August, namely: Northern and Eastern China had relatively more valid observations with numbers more than 80, while Western and Southwestern China had less valid observations with numbers less than 80. After that, the valid observation numbers in the southwestern parts of China began to increase from September, and the

spatial patterns of valid Landsat observations in China were similar in October–December, namely: Southern China had relatively less valid observations, as well as the western parts of the Xinjiang Autonomous Region and the northern parts of the Tibet Autonomous Region; while Northern, Northeastern, Eastern, and Southwestern China had more valid observations.

Given the variations of cloud covers, cloud shadows, and terrain shadows in different regions, we investigated the spatial patterns of valid Landsat observations within China along with the latitudes (15 N°–50 N°) by calculating the average number of valid observations in each one-degree latitude interval. Generally, the average number of valid observations in each one-degree latitude interval within China increased along with the latitudes, though it showed a decreasing trend along with the latitudes in high latitudes (>45 N°) in December and January (Figure S5).

Text S5. Spatial Distributions of Landsat Observations in China in Terms of Different Sensors

Figure S6 shows the spatial distributions of total and valid Landsat observations of L5, 7, and 8 within China from 1984 to 2017, respectively. Total and valid observations of different sensors showed different spatial patterns. For L5, Northern and Northeastern China had relatively more total (valid) observations with numbers more than 300 (240), while Southern and Western China (Western Xinjiang and Northern Tibet) had less. For L7, there were relatively more total (valid) observations in the Northern, Northeastern, and Western China with numbers more than 240 (140), while less in Southern China. For L8, only Western China had relatively more total observations with numbers more than 100. The spatial patterns of valid observations were different from that of total observations, namely: There were small differences in the spatial patterns of valid observations, except that the southern parts of China had relatively less valid observations with numbers less than 80.

By investigating the trends of total and valid observations along with the latitudes, we found that the average number of total and valid observations of the three sensors in each one-degree latitude interval within China increased along with the latitudes (Figure S6). It is notable that the average number of total and valid observations along with the latitudes kept relatively stable in latitudes higher than 35° N (Figure S7).

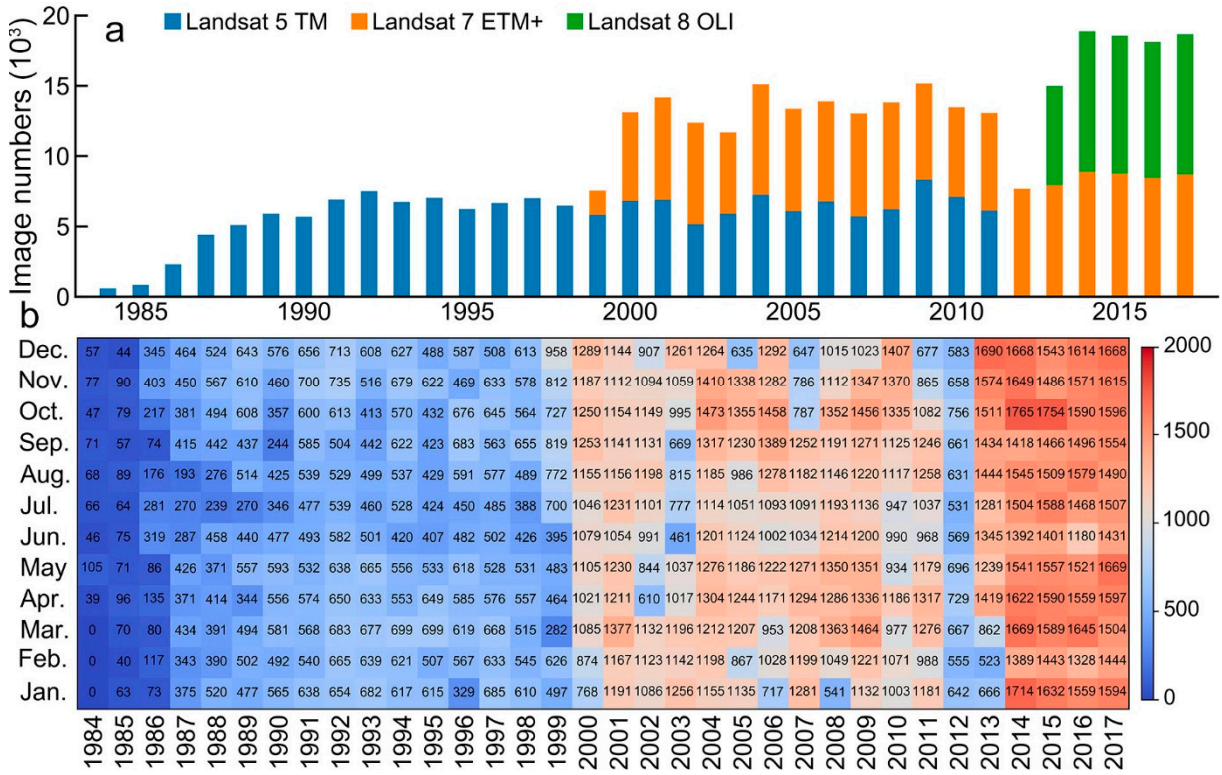

Figure S1. Yearly (**a**) and monthly (**b**) amounts of L5, 7, and 8 surface reflectance images in China from 1984 to 2017.

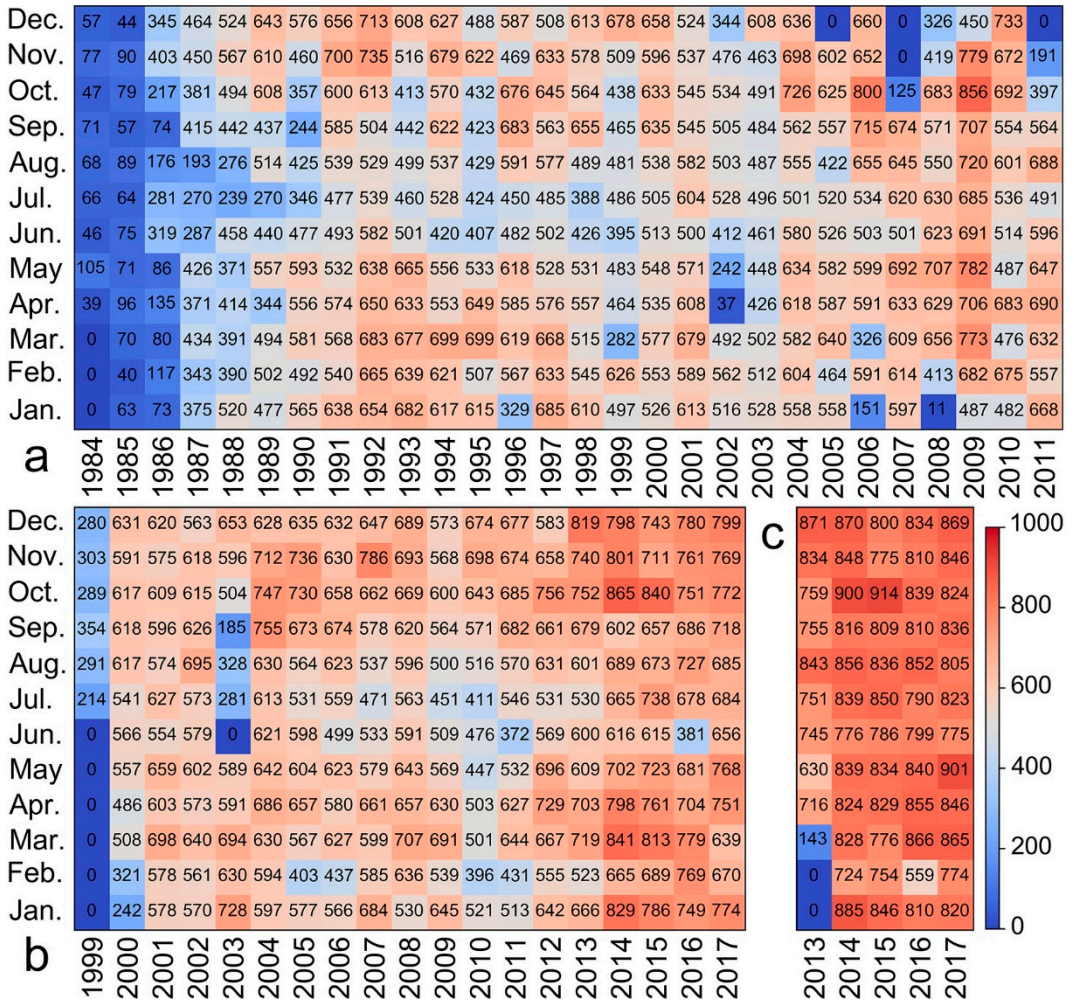

Figure S2. Monthly amounts of L5 (**a**), 7 (**b**), and 8 (**c**) surface reflectance images in China from 1984 to 2017.

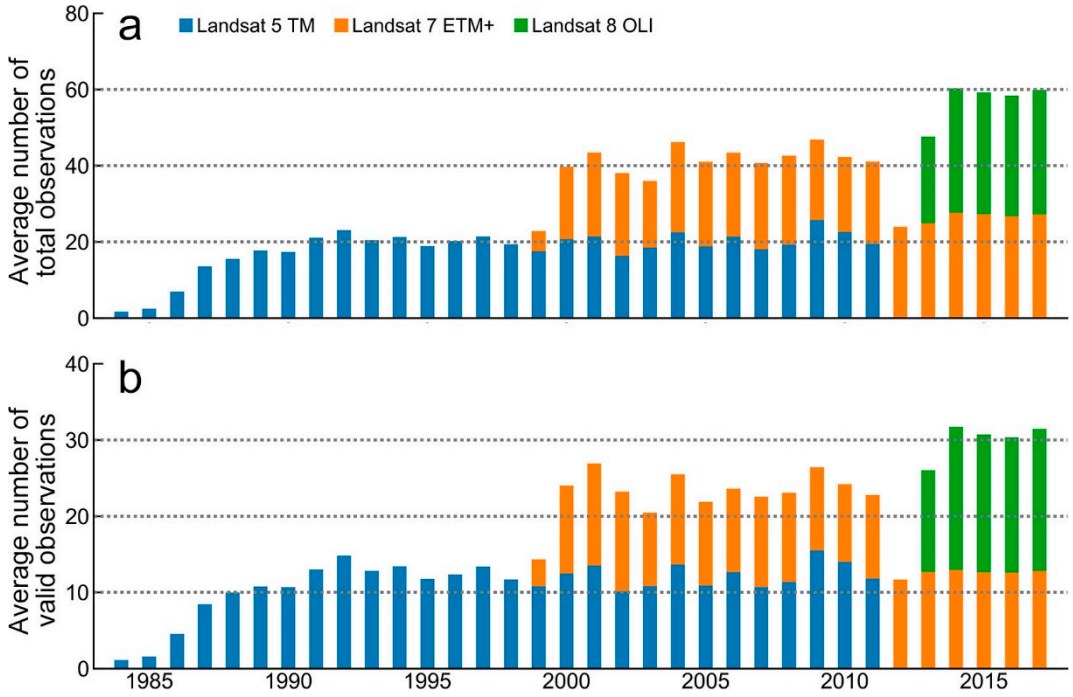

Figure S3. Yearly average number of total (**a**) and valid (**b**) observations of L5, 7, and 8 in China from 1984 to 2017.

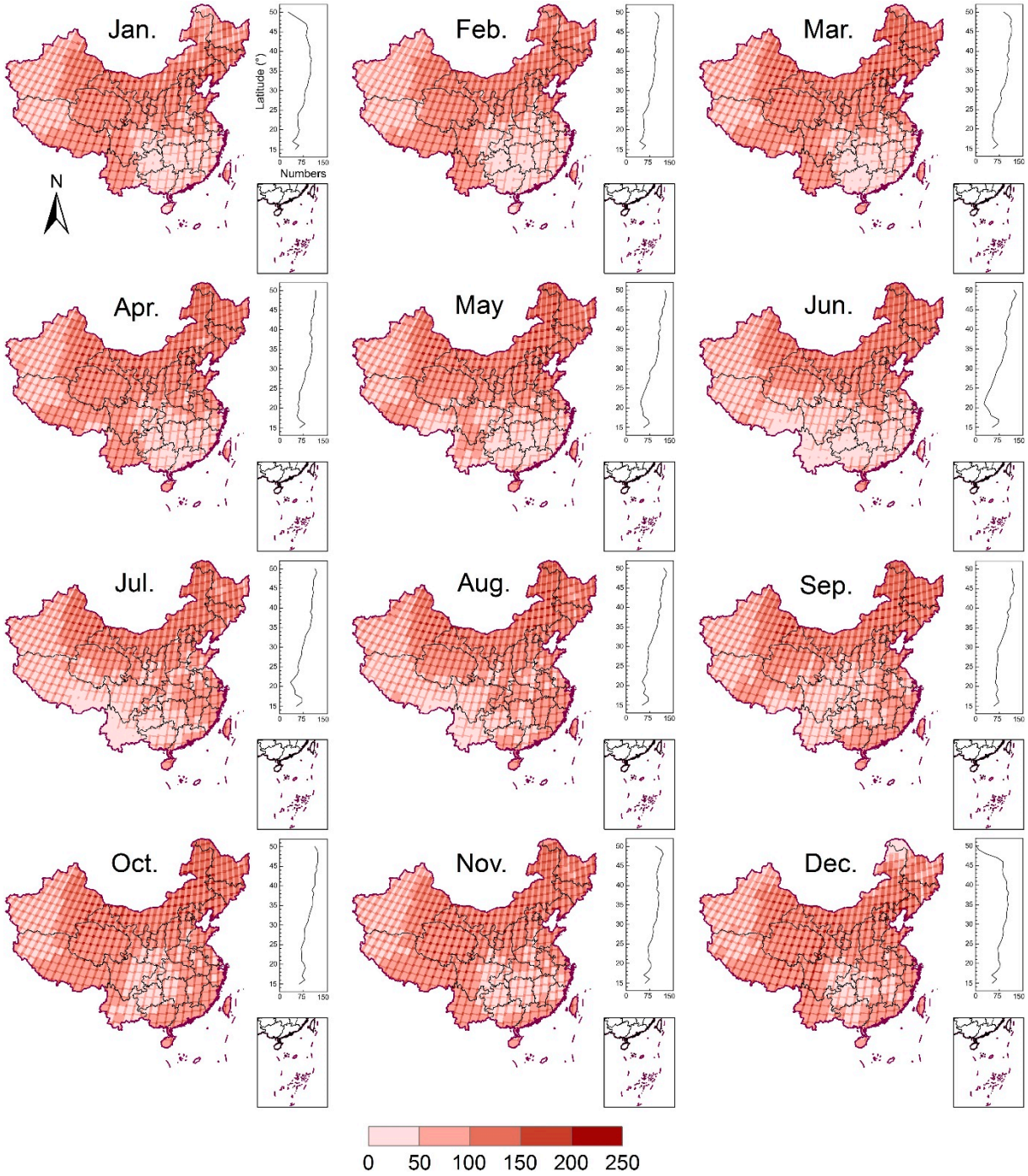

Figure S4. Spatial distributions of total Landsat observations in January–December. For each subfigure, the left part was the spatial distributions of total observations of L5, 7, and 8 in China in the specific month during 1984–2017, while the right part was the number of Landsat observations along with the latitudes.

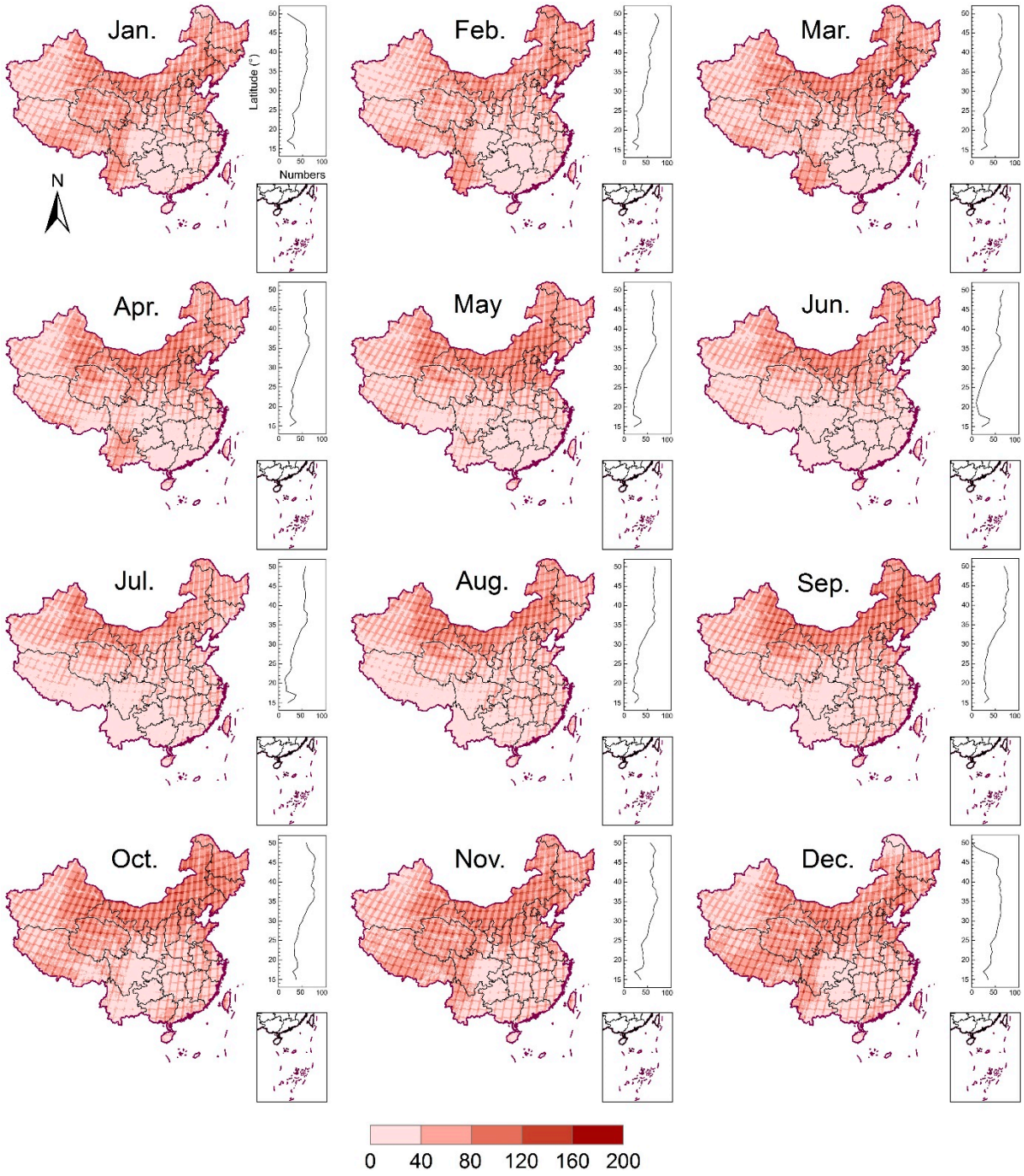

Figure S5. Spatial distributions of valid Landsat observations in January–December. For each subfigure, the left part was the spatial distributions of valid observations of L5, 7, and 8 in China in the specific month during 1984–2017, while the right part was the number of valid Landsat observations along with the latitudes.

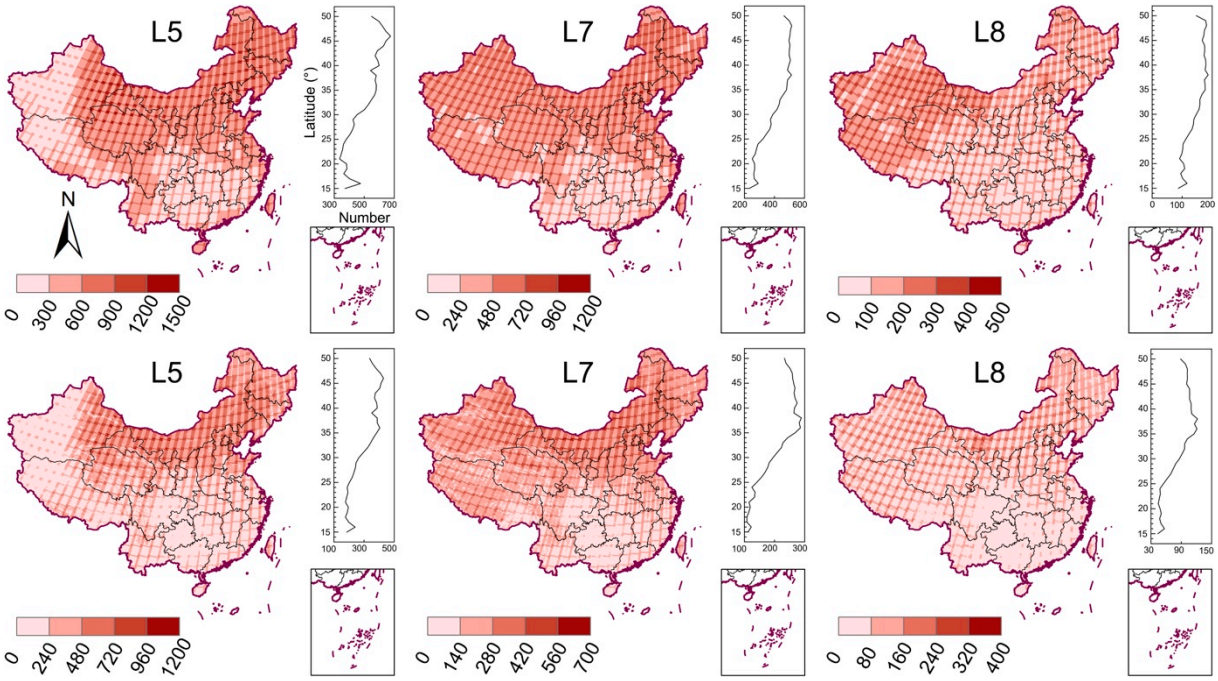

Figure S6. Spatial distributions of total (the first row) and valid (the second row) observations of L5, 7, and 8 in China from 1984 to 2017. For each subfigure, the left part was the spatial distributions of total (valid) observations in China during 1984–2017, while the right part was the total (valid) observation numbers along with the latitudes.

Google Earth Engine Code of This Study

```
// get the bites of data quality assessment band
function getQABits (image, start, end, newName) {
    // Compute the bits we need to extract.
    var pattern = 0;
    for (var i = start; i <= end; i++) {
       pattern += Math.pow(2, i);
    }
    // Return a single band image of the extracted QA bits, giving the band a new name.
    return image.select([0], [newName])
                  .bitwiseAnd(pattern)
                  .rightShift(start);
}

//remove bad observations (clouds, cloud shadows), for more info pls contact Corresponding author
function filterBadObs(img){

  // selection of Quality Assessment band
  var cfmask = img.select(['pixel_qa']);
  // mask of cloud
  var cloud_mask = getQABits(img.select('pixel_qa'),5,5,'cloud');
  // mask of cloud shadow
  var cloudShadow_mask = getQABits(img.select('pixel_qa'),3,3,'cloudShadow');
```

```
  var mask = ee.Image(0).where(cloud_mask.eq(0).bitwiseAnd(cloudShadow_mask.eq(0)),1);
  return mask
  }

function clipImage(image){
  return image.clip(region)
}

function count2Mean(year){

  //from Jun.1 to Oct.1
  var dataRange = ee.DateRange(ee.Date(year),ee.Date(year).advance(4,'month'))
  // surface reflectance image collection of Landsat 5/7/8
  var ImageCollectionL5 = ee.ImageCollection('LANDSAT/LT05/C01/T1_SR')
                          .filterBounds(region)
                          .filterDate(dataRange)
                          .sort('system:time_start')
                          .select(['B1','pixel_qa']);
  var ImageCollectionL7 = ee.ImageCollection('LANDSAT/LE07/C01/T1_SR')
                          .filterBounds(region)
                          .filterDate(dataRange)
                          .sort('system:time_start')
                          .select(['B1','pixel_qa']);
  var ImageCollectionL8 = ee.ImageCollection('LANDSAT/LC08/C01/T1_SR')
```

```
                    .filterBounds(region)

                    .filterDate(dataRange)

                    .sort('system:time_start')

                    .select(['B2','pixel_qa'],['B1','pixel_qa']);


  var
ImageCollection=ee.ImageCollection(ImageCollectionL5.merge(ImageCollectionL7).merg
e(ImageCollectionL8))  // Calculation of yearly percentages of Landsat pixels with at least
one valid observation

  // Removing invalid pixels

  var GoodObsers = ImageCollection.map(filterBadObs).select(0)

  // Calculating valid pixel numbers

  var validNum=GoodObsers.sum().select(0);

  var validExistOrNot = validNum.gt(0)


// Total numbers of Landsat pixels with at least one valid observation in China

  var areaProportion = validExistOrNot.reduceRegion({

      reducer: ee.Reducer.mean(),

      geometry: region,

      scale: 30,

      maxPixels:1e13,

      bestEffort:true,

      tileScale:16

    });


  var dict = {Area_Percentage: areaProportion};
```

```
  return ee.Feature(null,dict);
}

//Define region
var chinaBoundary = ee.FeatureCollection("users/2271832363/Subregion_IGSNRR");
var region = chinaBoundary.filter(ee.Filter.eq('Name','XJ'));

//Definition of year, from 1984 to 2017
var list = ee.List.sequence(0,33,1);
var list2Date = function (num){
  return ee.Date('1984-06-01').advance(num,'year'); // from 1984 to 2017
}
var year = list.map(list2Date);
print(year)

//Final Results
var fc = ee.FeatureCollection(year.map(count2Mean));

//Exporting the final results to csv file
Export.table.toDrive({
  collection:fc,
  description: 'XJ_1984_2017',
  fileFormat: 'CSV',
  folder:'Subregion'
});
```

```
//Exporting the spatial figure
// Export.image.toDrive({
//       crs: 'EPSG:4326',
//       image: result.clip(region),
//       description: "XJ_One_year",
//       scale: 30,
//       region: region,
//       folder:"Subregion",
//       maxPixels: 1.0E13
//       })
```